Fast and efficient transport of large ion clouds

M. R. Kamsap, J. Pedregosa-Gutierrez, C. Champenois,[*] D. Guyomarc'h, M. Houssin, and M. Knoop

Aix-Marseille Université, CNRS, PIIM, UMR 7345, 13397 Marseille, France

The manipulation of trapped charged particles by electric fields is an accurate, robust, and reliable technique for many applications or experiments in high-precision spectroscopy. The transfer of an ion sample between multiple traps allows the use of a tailored environment in quantum information, cold chemistry, or frequency metrology experiments. In this article, we experimentally study the transport of ion clouds of up to 80 000 ions over a distance of 20 mm inside a linear radio-frequency trap. Ion transport is controlled by a transfer function, which is designed taking into account the local electric potentials. We observe that the ion response is very sensitive to the details of the description of the electric potential. Nevertheless, we show that fast transport—with a total duration of 100 μs—results in transport efficiencies attaining values higher than 90% of the ion number, even with large ion clouds. For clouds smaller than 2000 ions, a 100% transfer efficiency is observed. Transport induced heating, which depends on the transport duration, is also analyzed.

PACS number(s): 37.10.Ty, 52.27.Jt, 07.77.Ka, 41.85.Ja

I. INTRODUCTION

Large clouds of ions find an interest in numerous applications ranging from frequency metrology to physical chemistry and the trapping of exotic species. In many cases, ion creation and manipulation are not made in the same place, and the reliable transport of the atomic sample is an essential ingredient of a successful experiment.

To our knowledge, the transport of rf-trapped ions has been studied only in the context of single ions [1–3] as it is a crucial issue for scalable architectures of quantum information processing (QIP) in ion traps. One of the main concerns in these experiments is to avoid heating issues during the transport [4]. In microtraps, the transport distances for a single ion are of the order of 100 μm. Care is taken to translate the ion in a quasiconstant potential well, which requires a large number of electrodes to tailor the trapping potential along the transport path. Speed is an additional issue which has to be taken into account, as shuttling ions between different sites is only a preparatory or intermediate task in a more sophisticated protocol and should not last longer than the computational gate.

Many-body transport is a concern for experiments with an ensemble of cold neutral atoms and Bose-Einstein condensates (BECs) which have been transported without heating, making use of shortcuts to adiabacity [5,6]. In [5] a cloud of a few 10^6 cold atoms is shuttled back and forth with an optical tweezer over a distance of 22.5 mm, in times as short as four trap oscillation periods. The use of an optical tweezer is very advantageous as it can be moved without deformation and the faster-than-adiabatic transport scheme relies on this nondeformation. The scheme designed in [6] allowed the authors to translate a cold gas in the noninteracting limit as well as a BEC and the noncondensed fraction by more than half a millimeter. The transport and decompression of the atomic sample was engineered using dynamics invariants. Because of the Coulomb repulsion, the method used for cold atoms cannot be extrapolated to ion clouds. For many experiments, adiabatic transfer is not a relevant solution. As for the trapping potentials in our experiment, the adiabatic transfer time is of the order of several tens of seconds, incompatible with a majority of precision experimental protocols.

In this paper, we address an out-of-equilibrium issue with the transport of ion clouds by the translation and deformation of the trapping potential. Our experiment is based on a macroscopic linear quadrupole rf trap with two trapping zones which can be controlled by dc voltages applied to three electrodes, storing ion clouds of a thousand up to a million ions. Such large traps are typically used in frequency metrology in the microwave domain [7], exotic ion studies [8], or experiments in physical chemistry [9]. Two different trapping zones are useful to keep one zone free from contact potentials induced by neutral atom deposit or to accumulate ions in one of the trapping zones. High number efficiencies are mandatory for transfer between traps, and rapid transport protocols can reduce dead times which are detrimental to frequency stability in the case of atomic clocks and to sample conservation in the case of short-lived species.

Our aim is to shuttle ions between separate trapping zones with a minimum of losses and as fast as possible. Even if this problem is inspired by the transport of single ions in microtraps, a different problem is studied here as the transported ensemble is a many-body system with long-range interaction. However, we can model the center-of-mass motion of the ion cloud by the trajectory of a single ion, and we therefore use the QIP transports as model systems.

This article is organized as follows: the experimental setup and techniques are presented in Sec. II. Section III is devoted to results and analysis of the transfer efficiency and the heating induced by the transport is analyzed in Sec. IV. Section V deals with the ion number effect for a specific transport duration with a focus on smaller clouds. The conclusion of this work can be found in Sec. VI.

II. DESCRIPTION OF THE EXPERIMENTAL SETUP AND PROTOCOL

A. Trapping and laser cooling

Calcium ions are trapped in a two-part linear quadrupole trap of inner radius $r_0 = 3.93$ mm which is designed to have

---
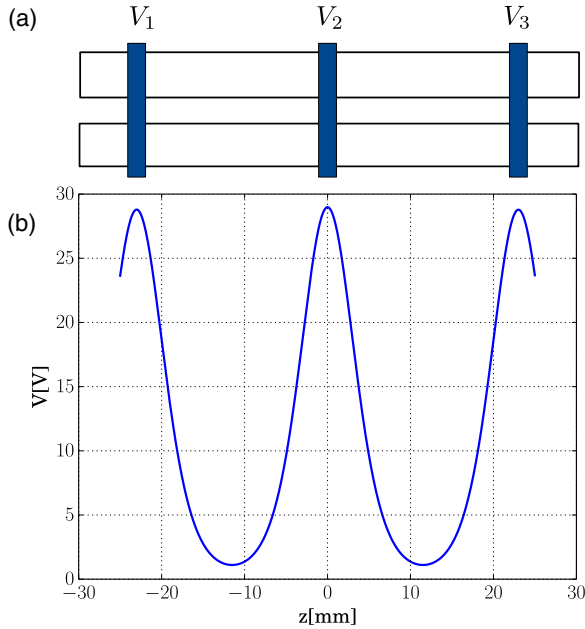
*caroline.champenois@univ-amu.fr

FIG. 1. (Color online) (a) Scheme of the experimental setup: the horizontal bars are the rf electrodes and the vertical ones stand for the dc electrodes. (b) Calculated dc potential along the trap axis if 1000 V are applied to each electrode. The distance between electrode centers is 23 mm and the thickness of each electrode is 2 mm.

reduced nonharmonic components in the trapping potential: the rf electrodes are four cylindrical rods of total length 58 mm, connected in a balanced way $[\pm(V_{RF}/2)\cos(\Omega t)]$ to the rf supply (no grounded electrodes). The rf frequency, $\Omega/2\pi$, is 5.23 MHz and the potential difference between neighboring electrodes oscillates with a peak-to-peak amplitude of 1045 V (if not mentioned otherwise) which gives a Mathieu parameter of $q_x = 0.15$, well within the adiabatic approximation regime where the rf trapping can be approximated by a static harmonic potential (the pseudopotential) with frequency $\omega_{x0} = q_x \Omega/(2\sqrt{2}) = 2\pi \times 277$ kHz.

Trapping along the symmetry axis, called z, is made by dc voltages applied to electrodes perpendicular to the rods. Three dc electrodes are located at equal distances along the rods, creating two distinct trapping zones (see Fig. 1). This double well configuration is used for accumulation in one of the wells before further transport of the ions to another trap, in line with the quadrupole one. The protocol for genuine accumulation of ions is described in detail in [10]. In order to laser cool the ions in both trapping regions using the same laser beam, the dc electrodes must leave the trap z-axis free, which justifies the open shape of the three of them. Their design, detailed in [11], results from a compromise between reduction of the nonharmonic contributions in the potential and of the screening effect induced by the rf rods.

The distance L between the center of adjacent dc electrodes is 23 mm and the trapping along the z axis results from the electric potential gradient of the sum of each electrode contribution. A solution of the Laplace equation by a finite difference method software (Simion [12]) gives the potential profile associated to each electrode of thickness 2 mm. The characteristic shape of the resulting potential wells along the

trap z axis are shown in Fig. 1. The effective potential well along the z axis, which can be estimated by the difference between the maximum and minimum total contribution, is lower than the dc voltage applied to the electrodes because of the screening by the rf electrodes [11] and by the overlapping of the potential profiles at the center of the trapping zones which offsets the potential minimum. The screening effect sets a limit to the axial trapping efficiency: for 1000 V applied to each electrode, the voltage calculated at the electrode center is 29 V for the central one and 28.8 V for the end electrodes whereas the minimal potential value is 1.16 V.

Calcium ions are produced by photoionization of neutral calcium atoms from an effusive beam crossing the trap axis perpendicularly in the horizontal plane. The photoionization process implies two photons and the first step (423 nm) is a resonant excitation tuned to select the most abundant isotope, ^{40}Ca [13,14]. The second photon, at 375 nm, takes the atomic system above the ionization threshold. Both beams copropagate along the trap axis. Ions are laser cooled by two collimated 397-nm beams on the $[4S_{1/2} - 4P_{1/2}]$ transition, of equal power (2 mW on a 2-mm $1/e^2$ diameter), counterpropagating along the trap axis. Once excited from the ground state, calcium ions can relax to a long-lived metastable state $[3D_{3/2}]$ from which they have to be repumped to maintain efficient laser cooling. This re-pumping process is assured by a 866-nm laser beam $[3D_{3/2} - 4P_{1/2}]$ of approximately 2.5 mW and 4 mm $1/e^2$ diameter which copropagates with one of the cooling lasers. Simultaneous ion creation and cooling allow us to trap clouds as large as several hundreds of thousands of ions. For the work presented here, we tuned the ion creation parameters to reach a cloud size of the order of 20 000 ions, which takes typically an integration time of 15 sec for laser powers of 80 μW at 423 nm and 4 mW at 375 nm. Ions are detected by their laser-induced fluorescence at 397 nm which is collected through a dedicated objective with antireflection coating and a high numerical aperture (Sill Optics, $f = 66.8$ mm, NA = 0.28).

B. Transport protocol

As pointed out in the Introduction, single-ion transport without heating is a major issue for the scalability of a trapped-ion quantum computer and is the subject of several experiments [1–3]. In these works, the authors characterize and compare different transport protocols with respect to the heating they induce on the ion motion. To guide us with our experiments, we have extrapolated these analyses for an ion cloud by using molecular dynamics (MD) simulations in [15]. We use the notations of previous work and we call $\phi_i(x,y,z)$ the electric potential created by the dc electrode i when 1 V is applied to it. Then, the total dc potential inside the trap can be expressed as [16]

$$\Phi(t,x,y,z) = \sum_{i}^{N} V_i(t)\phi_i(x,y,z) \qquad (1)$$

if $V_i(t)$ is applied to electrode i.

As the laser-cooled ions explore less than a tenth of the radial trap extension, we assume that the variations of the dc potential in the plane perpendicular to the trap axis are

not relevant, and we simply consider the on-axis evaluated function $\phi_i(x=0, y=0, z)$ we call $\phi_i(z)$. With our electrode geometry, the electric potential spatial distribution created on the axis is very well fitted around its maximum by the equation

$$f_i(z) = a_i \left(1 + \frac{(z-z_i)^2}{w_i^2} \right)^{-4} \qquad (2)$$

with z_i the position of the center of electrode i, $w_i = 8.9$ mm, and $a_{1,3} = 28.8$ mV and $a_2 = 29$ mV when 1 V is applied on the i electrode. The nonsymmetric environment of the trap explains the small variation between the a_i values. If $|z - z_i| = w_i$, $f_i(z) = a_i/16$ and we can consider that $2w_i$ is a good enough approximation of the effective width of the potential profile associated to each electrode. The two potential wells behave like $m\omega_z^2(z-z_c)^2/2$ in the first approximation. The value of ω_z deduced from a fit of the potential around its minimum is $2\pi \times 107.5$ kHz for $V_i = 1000$ V whereas a measurement by parametric excitation of the ion cloud [17] gives $2\pi \times 127$ kHz in zone 1 (which is the creation trap) and $2\pi \times 102$ kHz in zone 2. The difference between these last two values shows that the potential deduced from the calculation does not reproduce exactly the real potential experienced by the ions.

The transport protocol relies on the time variation of the V_i potential, designed to make the potential minimum obey a time profile $z_{\min}(t)$. This condition translates into

$$\left. \frac{\partial \Phi}{\partial z} \right|_{z_{\min}(t)} = 0. \qquad (3)$$

There are two local minima which meet each other when they reach the center of the central electrode and the challenge is to design a potential evolution which transfers the ions from the minimum in zone 1 to the minimum in zone 2 (see Fig. 1). In the following, we call $z_{\min}(t)$ the path we want the ions to follow and it can be written like [3]

$$z_{\min}(t) = g(t)[H(t) - H(t-t_g)] + LH(t-t_g) - L/2 \quad (4)$$

with L the shuttling distance, $g(t)$ the time profile of the transport, t_g its duration, and $H(t)$ the Heaviside step function. Guided by numerical results detailed in [15], we used for the experiments presented here the time profile described by

$$g(t) = \frac{L}{2} \left(\frac{\tanh[4(2t/t_g - 1)]}{\tanh(4)} + 1 \right), \qquad (5)$$

which is the most robust against transfer duration variations. These simulations also give evidence that the deformation of the trapping potential along the transport is responsible for the heating of the center-of-mass motion and of the ions' motion in the center-of-mass frame [15]. In our experimental setup, the distance between electrodes is larger than the effective width $2w_i$ of the potential they create [see Eq. (2)]. Therefore, because of the limitation of the applicable voltages, the axial potential is actually deformed during its translation. With the applied voltages V_i limited to 2000 V, and only three dc electrodes, we can simply change the depth of the effective harmonic potential but cannot compensate for its deformation.

In practice, the potential minimum is forced to obey the time profile $z_{\min}(t)$ if

$$V_2(t) = - \left. \frac{V_1(t)\phi_1'(z) + V_3(t)\phi_3'(z)}{\phi_2'(z)} \right|_{z_{\min}(t)} \qquad (6)$$

and the harmonic contribution of the resulting axial potential along the transport can be deduced by

$$\omega_z^2(t) = \frac{Q}{m} \left. \frac{\partial^2 \Phi}{\partial z^2} \right|_{z_{\min}(t)}, \qquad (7)$$

where Q is the ion charge and m its mass. In practice, the value of ω_z changes by several orders of magnitude along the transport.

Computing $V_2(t)$ through Eq. (6) requires us to know the potential profile created by each electrode to estimate the first-order derivative $\phi_i'(z)$. Single-ion experiments have shown the great sensitivity of the transport induced heating on the precise knowledge of the potential geometry. References [18,19] propose characterization methods for microtraps where a single ion or an ion crystal is a probe for the local electric field. The size of our trap and of the ion sample are not suited for this method, and we have hence based our calculations on $\phi_i(z) \simeq f_i(z)$ [see Eq. (2)]. Equation (6) leads to a discontinuity of $V_2(t)$ for $z_{\min}(t) = z_2$, the center of the electrode 2 where $\phi_2'(z_2) = 0$. To avoid this discontinuity, a constant relation between $V_1(t)$ and $V_3(t)$ is imposed, given by

$$V_3(t) = -V_1(t) \frac{f_1'(z_2)}{f_3'(z_2)}. \qquad (8)$$

In a perfectly symmetric device $V_3(t) = V_1(t)$ would solve the problem but any asymmetry in the electrode environment breaks this equality. The reader is referred to [15] for details about how to avoid discontinuities in numerical simulations.

In our experiments, V_1 and V_3 are not modified during the transport and the relative difference between V_1 and V_3 induced by the traps asymmetry is smaller than 0.1%. The initial value for $V_2(t)$ is chosen such that the minimum of the potential wells coincides with the geometric center of the traps. In practice, it also leads to a relative difference with V_1 smaller than 0.1% and we use V_1 as a value of reference to describe the dc trapping conditions.

III. TRANSFER EFFICIENCY FOR LARGE ION CLOUDS

A. Estimation of the number of ions

We are primarily interested in the transport efficiency as a matter of the relative number of ions passing from trapping zone 1 to zone 2. A precise quantitative study requires the measurement of the number of trapped ions, which is of the order of a few tens of thousands.

The ion's fluorescence signal is split between a photomultiplier and an intensified charge-coupled device camera. For fixed laser frequencies and trapping parameters, the fluorescence counting rate depends on the number of ions in the trap but also on their temperature. Because the transport can induce heating and ion loss, and because rf heating depends on the ion number and their temperature [20,21], there is no simple relation between the recorded fluorescence signal and the number of trapped ions. Indeed, we very often observe a

signal increase when the ion number has decreased, because of a smaller rf heating.

To develop a reliable quantitative diagnostic independent of the signal counting rate, we use the density characteristics of the liquid phase of an ion cloud. The thermal equilibrium state of a non-neutral plasma has been studied in detail by Dubin, O'Neil, and co-workers in the context of large ensembles in Penning traps (for a complete review, see [22]) and extrapolated to ions in rf-quadrupole traps [23,24]. One can show that in the cold fluid limit, a singly charged sample in a harmonic potential has a uniform density [25], bound by an ellipsoid of revolution where the density falls to zero on the scale of the Debye length. This results from the Boltzmann-Poisson equation in the low-temperature limit and for ions in a linear quadrupole trap the density depends only on the trapping pseudopotential [26]. This property, as well as the predicted aspect ratio of the ellipsoid [27], has been verified quantitatively very accurately for ions in a linear quadrupole trap in [28].

While in the gas phase during the transport, every ion ensemble is cooled to the liquid phase before and after transport in order to quantify the ion number with precision. The difference between liquid and gas phase is easily detected by the variation in the fluorescence level [28]. The calculated density in the liquid phase is 1.40×10^5 mm^{-3} and for a typical temperature of 100 mK, the Debye length is 1.85 μm, which fits within two pixels on the camera with an optical magnification of the order of 13. The Debye length is negligible compared to the cloud size and we consider a uniform density all over the cloud in the liquid phase. We checked that, once the ellipsoid is formed by laser cooling, the measured dimensions for the ellipse are constant for different temperatures and the slight modification of the Debye length has no impact on the measured values. A software has been developed which automatically fits and extracts the dimensions of an ellipse from the recorded picture of the collected fluorescence (see the Appendix).

B. From one local minimum to the other

In a first step, we study the transfer of ions from one trapping zone to the other, depending on the transfer duration t_g for given trapping parameters. Bandpass limitations of the dc supplies prevent us from investigating transport durations shorter than 80 μs. All the experiments were done with an ion cloud in the gas phase with a typical size ranging 1000–20 000 ions and an estimated temperature ranging 1–10 K. For some of the studied transport durations, we checked that the transport efficiency is independent of the ion number as long as this number is larger than 2000. For clouds smaller than 2000, the efficiency is higher than for larger clouds and can reach 100%. A focus on smaller cloud transfer is presented in Sec. V. As our detection is based on the observation of induced fluorescence, the cooling laser beams remain applied during the transport. For transport durations ranging 100–500 μs, we compared the transport efficiency with and without the cooling laser during transport. The observed differences were only of the order of a few % showing that the cooling effect does not play an important role. Indeed, the capture range of the Doppler laser cooling is 9.2 m/s, smaller or far smaller than the average shuttling velocity which ranges 20–200 m/s.

Figure 2 shows the fraction of ions leaving the trapping zone 1 for t_g between 80 μs and 2.6 ms. The first major observation is that the number of leaving ions depends strongly on t_g, alternating between nearly 0 and 100% several times before these oscillations are damped. Changing the axial trapping potential by increasing the initial value of all three dc voltages shifts these oscillations with t_g and increases the number of observed oscillations. If the same protocol is applied to a smaller ion cloud (typically 1000 ions and smaller), oscillations are also observed with identical temporal imprint, excluding a number dependent effect. A possible explanation for this interchange between a high and low transfer probability is the oscillation of the ion cloud from zone 1 to zone 2 and
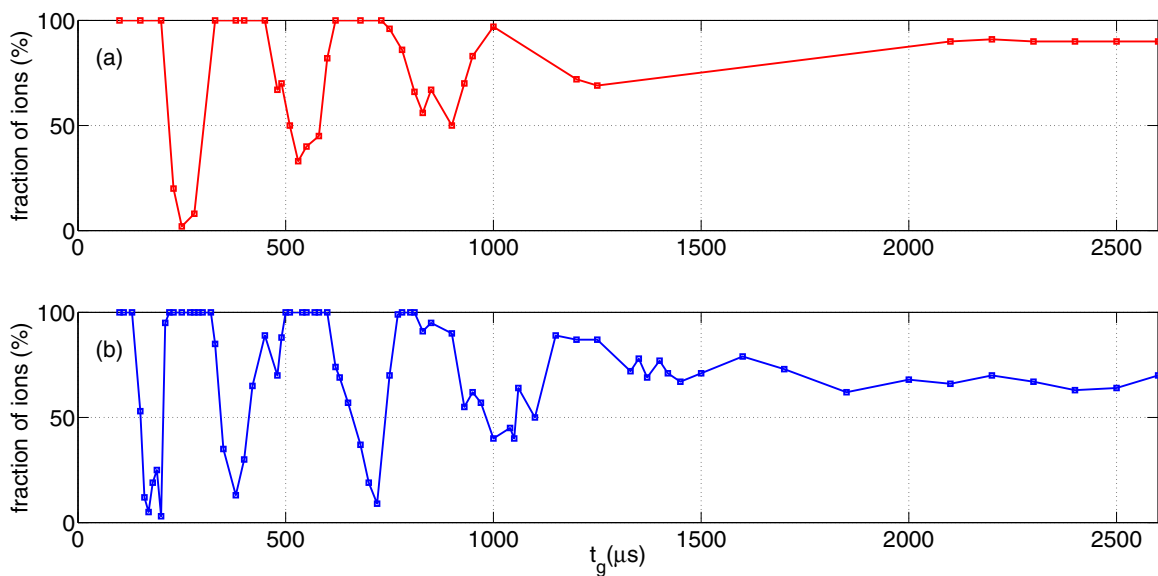
FIG. 2. (Color online) Fraction of ions leaving the trapping zone 1 vs the transport duration t_g for different on-axis dc voltages: (a) $V_1 = 600$ V, (b) $V_1 = 1200$ V. Only V_2 is changed during the transport. The cloud initial size ranges 5000–20 000. Each point is the result of one experiment. The lines are a guide to the eye.
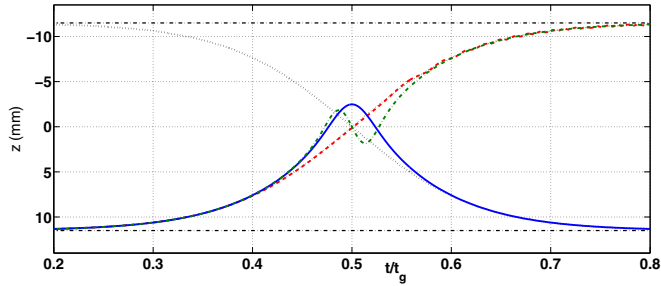
FIG. 3. (Color online) Single-ion trajectories, initially at rest, computed by MD vs the relative time elapsed during the transfer. The trajectories are computed in the potential grid provided by the Simion software, based on our electrode geometry, when $V_2(t)$ obeys Eq. (6) computed with $\phi_i(z) = f_i(z)$. Red dashed line: $t_{g1} = 189\ \mu$s; solid blue line: $t_{g2} = 884\ \mu$s; green dot-dashed line: $t_{g3} = 1621\ \mu$s. The black dotted lines are the positions of the two potential minima along the transfer (one is hidden behind the red curve). Horizontal dash-dotted lines indicate the positions of the centes of the traps.

their return to trapping zone 1 before the transport function is completed.

For transport durations longer than 1 ms, the fraction of transferred ions reaches a stationary value. In an ideal, symmetric system this value is expected to be 50%. In our dual trap, an asymmetry, very probably due to contact potentials in trapping zone 1, can be responsible for this imbalance in ion repartition for long transport durations.

To get more insight into this issue, we use a MD simulation to compute the trajectory of a single ion, as a good approximation of the center-of-mass motion [15]. Actually, the results of this simulation depend on the potential used for calculating, first, the wave form of the transfer function $V_2(t)$ and second, the ion trajectory. If for both calculations, the same description of the potential is used, the probability for the ion to be transferred to zone 2 is unity, for all explored t_g (values smaller than 10 s). To come closer to the experimental situation, we keep the same wave forms $V_2(t)$ as designed by

$$V_2(t) = -\left. \frac{V_1(t)f_1'(z) + V_3(t)f_3'(z)}{f_2'(z)} \right|_{z_{\min}(t)} \quad (9)$$

with the f_i defined by Eq. (2), but integrate the equation of motion in the original potential grid calculated by the finite difference method software, Simion [12].

In this condition, the calculated probability to transfer the ion to trapping zone 2 oscillates between 0 and 1, depending on the transfer duration, like observed in the experiment. We attribute this behavior to the discrepancy between the potential assumed to compute the wave form of the transfer function $V_2(t)$ and the one used to compute the trajectories. The main difference with the experimental results is that the oscillations do not smear out for long transport, which we attribute to an ion number effect. Like shown in [15], for longer transport, the spreading of the cloud starts to play a role and following the center-of-mass motion is not sufficient to explain the transfer efficiency of a cloud. Several examples of ion trajectories are plotted in Fig. 3 to compare successful and failed transfer. For t_{g1}, the ion trajectory follows the potential minimum from trapping zone 1 to zone 2. For longer transfer durations, the ion

is ahead of the potential minimum and for t_{g2}, makes a U-turn in zone 2 before ending up in zone 1, as assumed previously. For even longer transfer times (t_{g3} in Fig. 3), the calculated trajectory shows a U-turn in zone 2, followed by a U-turn in zone 1, to finally have an ion efficiently transferred to zone 2. Longer transfer durations give rise to an increasing number of U-turns which results in an oscillation between trap 1 and trap 2 for the final ion position.

The time scale of oscillations of the final ion position is typically 200 μs in the experiments, a shorter value than in the simulations. This can be explained by a larger difference than in the simulations between the potential assumed to compute the $V_i(t)$ and the one experienced by the ions in the trap. Precise description of the local trapping field is an essential factor in transport experiments, as has been evidenced before [29]. In single-ion experiments the field can be precisely mapped, improving the match between real and assumed potential. In a large-scale experiment, however, it seems unrealistic to generate a precise map of the complete electric field seen by the ion cloud along its transport. Nevertheless, the experimental results show that it is still possible to force the ion to transfer even if the corresponding absolute time values cannot be exactly foreseen. The next step in the transport efficiency analysis is to look at how many ions effectively settle in the other part of the trap.

C. Transport induced ion loss

The next step in our transport efficiency characterization is to check that all ions leaving zone 1 are trapped in zone 2 by the end of the transport protocol. As only a single fluorescence collecting optics is used in the experiment, the precise characterization of the transfer efficiency requires that the ions are transferred back to their original position for a comparison between the cloud sizes. To circumvent this drawback and be able to estimate the one-way transfer efficiency, we identified a transfer protocol that is efficient enough to serve as a standard operation. This is the case for the transfer of 100 μs duration. As mentioned previously, the transfer efficiency depends very little on the ion number as long as this number is larger than 2000 ions. This efficiency was estimated from several consecutive transport protocols to be of the order of 90% for 100 μs. Ions remain laser cooled in zone 1 for 5 s before next step, assuring a recooling of the cloud. By maintaining an identical protocol for the zone 2 to zone 1 transfer, we can observe the dependence of the zone 1 to zone 2 transfer efficiency as a function of the transport duration, as shown in Fig. 4. The largest two-way transfer efficiency is as high as 90% and is observed for a transport made of two consecutive 100-μs transport protocols. Increasing the duration of a transport protocol does not result in a higher transfer efficiency. This is consistent with the numerical simulations detailed in [15] which show how the cloud spreading makes long transport durations inappropriate for large clouds.

The results of Fig. 4 show oscillations of the fraction of transferred ions with the transfer duration, out of phase with the fraction of ions not leaving trapping zone 1. The ion number budget summing up to values below 1 evidences transfer-induced ion loss, which depends on the transfer
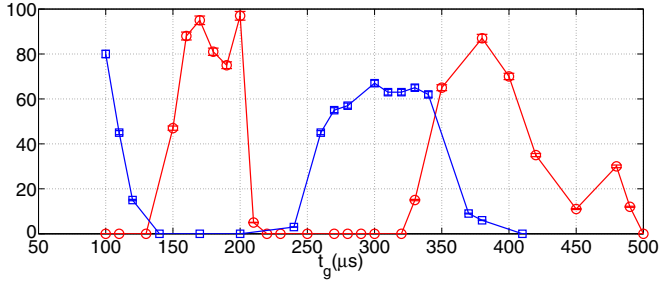
FIG. 4. (Color online) Ions are transferred from zone 2 to zone 1 by a transfer protocol of duration 100 μs (efficiency larger than 90%) and remain laser cooled in zone 1 for 5 s before next step. Blue squares: fraction of ions transferred back to zone 2 by a transfer protocol of duration t_g. Red dots: fraction of ions not leaving zone 1 after a transfer protocol of duration t_g. Including ion losses both curves should add up to 1. The dc voltages are 1200 V (the lines are a guide to the eye).

duration. In the next section, we quantify the transfer-induced cloud heating to look for possible correlations with the ion loss.

IV. EXCITATION OF MOTION

The transport-induced motional excitation has a signature on the time evolution of the fluorescence. All lasers are on and their frequencies are kept constant during the experiment and the temporal evolution of the fluorescence directly after the transport depends on the Doppler effect, which depends on the ion velocity along the trap axis. Heating may occur during transport; in that case, a recooling phase can be observed. The time T_f required for the fluorescence rate to reach its stationary value after a transfer operation is plotted in Fig. 5. Laser cooling competes with rf heating which depends on the temperature and the ion number [21]. To use the recooling time as an indicator of the temperature after transport, the experiments must be done with a constant number of ions. In that case, the chosen transport durations for this experiment are larger than the one explored for Fig. 4 to make sure that a large and nearly steady proportion of the ion cloud arrives in zone 2 (see Fig. 2). Let us mention that for the particularly
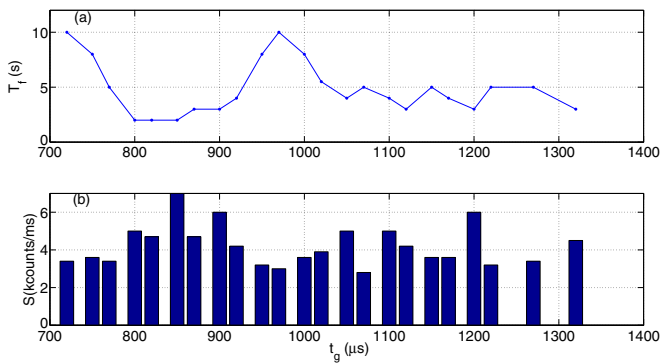

FIG. 5. (Color online) (a) Time T_f it takes for a transported cloud in zone 2 to recover its maximal fluorescence rate after a transfer from zone 1 of duration t_g. (b) Value of this maximal signal. The dc initial voltages are 1800 V.

efficient transport with $t_g = 100$ μs, the recooling time T_f ranges between 1 and 2 s.

For transport durations longer than 700 μs, the recooling time T_f can vary from short (2 s) to long (10 s) times which shows that the Doppler broadening induced by the transport depends on the duration of the transport and does not simply decrease with time. Also in Fig. 5(b) is plotted the maximum fluorescence rate, which can be considered as a crude indication for the ion number. The graph confirms that a fast recovery of the signal is not due to a lower number of ions. As seen on the comparison of the two curves of Fig. 5, the amplitude variations of the signal are anticorrelated with the recovery time of the fluorescence rate. In a hand-waving argument, we can interpret the time T_f as an indicator for the motional excitation, and deduce from this figure that a larger number of ions is efficiently transferred to trapping zone 2 when this excitation is low, which is the case for $t_g = 100$ μs. When a smaller rf amplitude is used (which results in $q_x = 0.12$ instead of 0.15), the signal recovery time can be as small as 200 ms and does not exceed 5 s, showing that the ion velocities are less modified by the transport process. The global increase of the signal recovery time with the rf amplitude can be interpreted by nonlinear terms in the equation of motion coupling the motion along the radial and axial directions, and giving rise to rf heating of the motion. In our experimental context, the axial potential is deformed and the nonharmonic contributions are non-negligible when the potential minimum crosses the site of the central electrode. The anharmonic contributions induce a coupling between the center-of-mass motion and the motion in the center-of-mass frame which is responsible for an increase of the kinetic energy of the center of mass. MD simulations of the transport of an ion cloud [15] showed that this contribution increases with the transport duration, as the cloud spreads further. The experimental results do not show such a behavior for the time scale explored, leaving the cause of duration-dependent cloud heating unexplained.

V. TRANSFER EFFICIENCY VERSUS ION NUMBER

We analyze the ion number effect for the transport duration which gives the highest two-way transport efficiency. In the described case, the protocol uses transport functions of duration $t_g = 100$ μs. Figure 6 shows that for clouds of less than 5000 ions, the round-trip transfer efficiency increases with shrinking cloud size and can reach unity for ensembles of less than 2000 ions. We assume that this size effect is due to
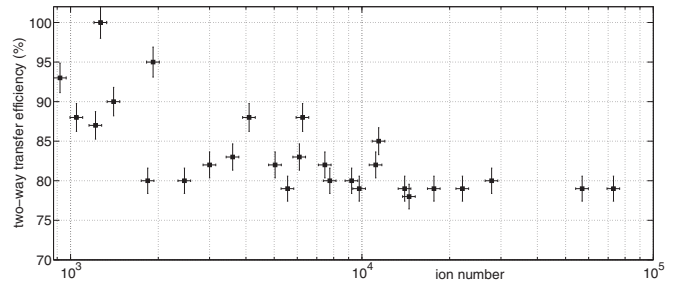

FIG. 6. Ratio of the number of ions after shuttling back and forth from trapping zone 2 with two identical transport protocols, vs the initial number of ions.

the spatial spreading of the cloud. This figure also shows that for this chosen transport function, the round-trip efficiency for shuttling is typically higher than 80%. These high ratios can be realized with ion clouds of up to 10^5 ions. This very fast and efficient shuttling is in particular interesting for experiments in frequency metrology, as for example [7].

VI. CONCLUSION

We have experimentally studied the transport of ion clouds in a macroscopic rf trap for cloud sizes as large as several tens of thousands ions. This transport is controlled by the potential applied to a single central dc electrode splitting the trap into two zones. We have used a time profile for the transport function which is designed for single-ion shuttling, and which can result in the transfer of the complete ion cloud. Our experimental results and their comparison with MD simulations show that the mismatch between the potential assumed for the design of the transfer function and the actual dc potential experienced by the ions explains the very different transfer efficiencies observed for various transport durations. This transfer efficiency can drop from 90% to 0 by a change in the transfer duration by 100 μs, and we observe that the shortest transfer durations give the best transfer efficiencies. An oscillatory behavior on the same time scale can also be observed for transfer-induced heating.

The observed oscillations in the transfer efficiency can be shifted with the transport duration by choosing different trapping parameters, and the minimum heating can be lowered by using smaller rf amplitudes. It is therefore possible to find conditions for which the transfer efficiency is high and the motional excitation is low for the same transfer duration. For clouds containing less than 2000 ions, 100 ($\pm$1.5)% transfers can be achieved. This is another step approaching our objective which is to transfer large ion clouds with 100% efficiency without heating. Our best results for clouds larger than 5000 ions are transfers of 92%.

As the transfer efficiency depends on small variations of the potential profile, its dependence with the transport duration varies with the sense of transport. It is then possible to choose a "no-return" parameter set, where ions are transferred with a very high probability from a first trap to a second trap, but at the same time they do have an extremely low probability to leave the second trap. This asymmetric protocol allows us to implement a true accumulation process, whose experimental realization is described in [10].

APPENDIX: DETERMINATION OF THE NUMBER OF IONS IN A CLOUD

Measuring the efficiency of ion transport relies on a trustworthy and precise method to count them. Our analysis is based on the cold fluid model developed by Dubin *et al.* for non-neutral plasma [22].

The first step is to define the contour of the fluorescence signal, imaged on a camera, when the ions are in the liquid phase. This requires the definition of a threshold for the signal, independent from the number of photons scattered per ion. The threshold criteria is provided by the analysis of the section of the signal along one pixel line across the image. The derivative of the signal with respect to the pixel position shows two sharp extrema, X_1 and X_2 at the ellipse border (see Fig. 7). Their position falls in the same pixel as the one chosen by a visual
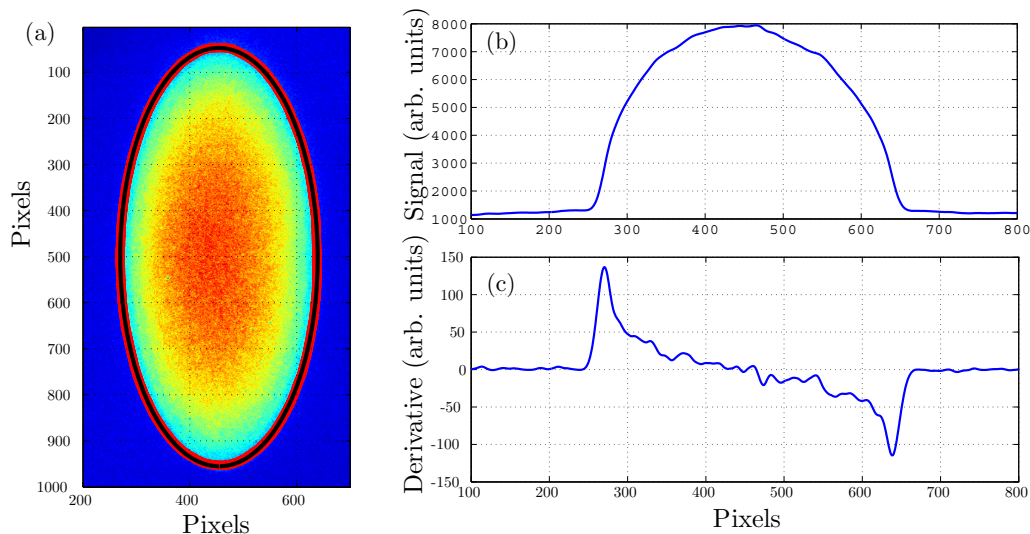

FIG. 7. (Color online) (a) Example of the picture of an ion cloud (dimensions in pixels) in the liquid phase with the fit of the contour (exposure time 0.5 s). The trap axis and laser propagation direction are vertical. (b) Smoothed section of the signal along the short axis of the ellipse, and (c) its derivative.

fit and does not depend on the absolute level of the signal. As some of the ellipse pictures are longer than the camera detector, we base our protocol on a section located approximately on the small axis and define the level threshold as the mean signal $[S(X_1) + S(X_2)]/2$.

The second step is to fit the contour by an ellipse equation, including a possible angle between the ellipse semiaxis and the detector rows. This is done through a two-dimensional (2D) fit subroutine and produces a fit which falls in the same pixels as the original contour, which confirms the ellipsoid shape of the cloud. To validate our fit procedure, for the same ion cloud, simply deformed by changing the trapping parameters, we use the two calculated semiaxis lengths R_e and L_e to estimate the ellipse aspect ratio $\rho_e = R_e/L_e$ and volume $V_e = 4\pi R_e^2 L_e/3$ extracted from experimental data. We can compare the aspect ratio with the expected one, deduced from the effective pseudopotential $\rho = f(\omega_z/\omega_r)$ by an equation demonstrated in [27] and experimentally confirmed in [30]. More precisely, as a test for our analysis method, we measure the shift δ_L between the length deduced from the fit and the one deduced by the fitted radius, assuming a known aspect ratio: $\delta_L = (L_e - R_e/\rho)$. Furthermore, we can check that the volume modifications obey what is expected from the density $n(\mathbf{r})$ at low temperature:

$$n(\mathbf{r}) = \epsilon_0 \Delta \Psi_{pp}(\mathbf{r})/Q, \tag{A1}$$

where $\Psi_{pp}(\mathbf{r})$ is the harmonic pseudopotential, characterized by

$$\Psi_{pp}(\mathbf{r}) = \frac{1}{2Q}m(\omega_x^2 - \omega_z^2/2)(x^2 + y^2) + \frac{1}{2Q}m\omega_z^2 z^2 \quad \text{(A2)}$$

which leads to a uniform density $n(\mathbf{r}) = n_0 = \epsilon_0 2m\omega_x^2/Q^2$. As we want to reach a 1% level accuracy in relative volume

estimation, we have to go beyond the first-order adiabatic approximation. By expanding the calculation of the coefficient in the Mathieu solutions to the second order in (q_x^2, a_x), one can show that

$$\omega_x^2 = \omega_{x0}^2 \left(1 + \frac{q_x^2}{2} + a_x\right). \tag{A3}$$

In our case, a_x is induced by the z-axis trapping voltage V_{dc}, $a_x = -2\omega_z^2/\Omega^2$, and with our operating parameters, the correction is in the 1% range. Taking that into account, for the same rf amplitude but different dc voltages, we observe for the same cloud in zone 2 that the length shift remains smaller than $\pm1\%$ and the volume fluctuations are lower than 1%. In zone 1, we observe volume fluctuations that can reach 6%, far larger than the length shift fluctuations δ_L which remain in the $\pm1\%$ range. We attribute this difference to the contact potential, identified in zone 1 and induced by calcium deposits on the quadrupole rods, in front of the calcium oven. For different trapping parameters, the cloud is displaced in the trap, giving an optical image with a slightly different size. This is in particular true when the rf amplitude is changed and where apparent ion numbers can vary by 10%. For constant trapping parameters, like used for estimating the relative number of ions after a transport cycle, the uncertainty on the volume is $\pm1\%$ for zone 2 and $\pm1.5\%$ for zone 1 (6σ confidence). Precise investigations of transport efficiencies in terms of ratios of ion numbers only require measurement of the volume of the ellipses as we compare cold clouds with identical density. As for an estimation of the number of ions in a cloud, the fluctuations of the apparent particle number for the same cloud, when it is deformed and shifted, lead us to fix a 5% uncertainty on the absolute number, with a negligible contribution from the uncertainty induced by the optical magnification.

---

[1] R. Reichle, D. Leibfried, R. Blakestad, J. Britton, J. Jost, E. Knill, C. Langer, R. Ozeri, S. Seidelin, and D. Wineland, Fortschr. Phys. **54**, 666 (2006).

[2] S. Schulz, U. Poschinger, K. Singer, and F. Schmidt-Kaler, Fortschr. Phys. **54**, 648 (2006).

[3] D. Hucul, M. Yeo, S. Olmschenk, C. Monroe, W. K. Hensinger, and J. Rabchuk, Quantum Inf. Comput. **8**, 501 (2008).

[4] K. Wright, J. M. Amini, D. L. Faircloth, C. Volin, S. Charles Doret, H. Hayden, C.-S. Pai, D. W. Landgren, D. Denison, T. Killian, R. E. Slusher, and A. W. Harter, New J. Phys. **15**, 033004 (2013).

[5] A. Couvert, T. Kawalec, G. Reinaudi, and D. Guéry-Odelin, Europhys. Lett. **83**, 13001 (2008).

[6] J.-F. Schaff, P. Capuzzi, G. Labeyrie, and P. Vignolo, New J. Phys. **13**, 113017 (2011).

[7] J. Prestage and G. Weaver, Proc. IEEE **95**, 2235 (2007).

[8] F. Herfurth, in *14th International Conference on Electromagnetic Isotope Separators and Techniques Related to their Applications* [Nucl. Instrum. Methods Phys. Res., Sect. B **204**, 587 (2003)].

[9] R. Wester, J. Phys. B **42**, 154001 (2009).

[10] M. R. Kamsap, C. Champenois, J. Pedregosa-Gutierrez, M. Houssin, and M. Knoop, Europhys. Lett. **110**, 63002 (2015).

[11] J. Pedregosa, C. Champenois, M. Houssin, and M. Knoop, Int. J. Mass Spectrom. **290**, 100 (2010).

[12] http://www.simion.com.

[13] S. Gulde, D. Rotter, P. Barton, F. Schmidt-Kaler, R. Blatt, and W. Hogervorst, Appl. Phys. B **73**, 861 (2001).

[14] D. M. Lucas, A. Ramos, J. P. Home, M. J. McDonnell, S. Nakayama, J.-P. Stacey, S. C. Webster, D. N. Stacey, and A. M. Steane, Phys. Rev. A **69**, 012711 (2004).

[15] J. Pedregosa-Gutierrez, C. Champenois, M. R. Kamsap, and M. Knoop, Int. J. Mass Spectrom. **381-382**, 33 (2015).

[16] K. Singer, U. Poschinger, M. Murphy, P. Ivanov, F. Ziesel, T. Calarco, and F. Schmidt-Kaler, Rev. Mod. Phys. **82**, 2609 (2010).

[17] C. Champenois, M. Knoop, M. Herbane, M. Houssin, T. Kaing, M. Vedel, and F. Vedel, Eur. Phys. J. D **15**, 105 (2001).

[18] G. Huber, F. Ziesel, U. Poschinger, K. Singer, and F. Schmidt-Kaler, Appl. Phys. B **100**, 725 (2010).

[19] M. Brownnutt, M. Harlander, W. Hänsel, and R. Blatt, Appl. Phys. B **107**, 1125 (2012).

[20] V. L. Ryjkov, X. Z. Zhao, and H. A. Schuessler, Phys. Rev. A **71**, 033414 (2005).

[21] Y. S. Nam, E. B. Jones, and R. Blümel, Phys. Rev. A **90**, 013402 (2014).

[22] D. H. E. Dubin and T. M. O'Neil, Rev. Mod. Phys. **71**, 87 (1999).

[23] D. Dubin, Phys. Fluids B **5**, 295 (1993).

[24] J. Schiffer, M. Drewsen, J. Hangst, and L. Hornekær, Proc. Natl. Acad. Sci. USA **97**, 10697 (2000).

[25] S. A. Prasad and T. M. O'Neil, Phys. Fluids **22**, 278 (1979).

[26] C. Champenois, J. Phys. B **42**, 154002 (2009).

[27] L. Turner, Phys. Fluids **30**, 3196 (1987).

[28] L. Hornekær and M. Drewsen, Phys. Rev. A **66**, 013412 (2002).

[29] H. A. Fürst, M. H. Goerz, M. M. U. G. Poschinger, S. Montangero, T. Calarco, F. Schmidt-Kaler, K. Singer, and C. P. Koch, New J. Phys. **16**, 075007 (2014).

[30] L. Hornekær, N. Kjærgaard, A. M. Thommesen, and M. Drewsen, Phys. Rev. Lett. **86**, 1994 (2001).